Published in final edited form as:

Immunity. 2016 August 16; 45(2): 374–388. doi:10.1016/j.immuni.2016.07.009.

The Tumor Microenvironment Represses T Cell Mitochondrial Biogenesis to Drive Intratumoral T Cell Metabolic Insufficiency and Dysfunction

Nicole E. Scharping[1,2], **Ashley V. Menk**[1], **Rebecca S. Moreci**[1], **Ryan D. Whetstone**[1,2], **Rebekah E. Dadey**[1,2], **Simon C. Watkins**[2,3], **Robert L. Ferris**[1,2,4], and **Greg M. Delgoffe**[1,2,*]

[1]Tumor Microenvironment Center, University of Pittsburgh Cancer Institute, Pittsburgh, PA 15261, USA

[2]Department of Immunology, University of Pittsburgh, Pittsburgh, PA 15261, USA

[3]Department of Cell Biology, University of Pittsburgh, Pittsburgh, PA 15261, USA

[4]Department of Otolaryngology, University of Pittsburgh, Pittsburgh, PA 15261, USA

SUMMARY

Although tumor-specific T cells recognize cancer cells, they are often rendered dysfunctional due to an immunosuppressive microenvironment. Here we showed that T cells demonstrated persistent loss of mitochondrial function and mass when infiltrating murine and human tumors, an effect specific to the tumor microenvironment and not merely caused by activation. Tumor-infiltrating T cells showed a progressive loss of PPAR-gamma coactivator 1α (PGC1α), which programs mitochondrial biogenesis, induced by chronic Akt signaling in tumor-specific T cells. Reprogramming tumor-specific T cells through enforced expression of PGC1α resulted in superior intratumoral metabolic and effector function. Our data support a model in which signals in the tumor microenvironment repress T cell oxidative metabolism, resulting in effector cells with metabolic needs that cannot be met. Our studies also suggest that modulation or reprogramming of the altered metabolism of tumor-infiltrating T cells might represent a potential strategy to reinvigorate dysfunctional T cells for cancer treatment.

Abstract

*Correspondence: gdelgoffe@pitt.edu.

SUPPLEMENTAL INFORMATION

Supplemental Information includes seven figures and Supplemental Experimental Procedures and can be found with this article online at http://dx.doi.org/10.1016/j.immuni.2016.07.009.

AUTHOR CONTRIBUTIONS

N.E.S. performed experiments, performed data analysis, and helped write the manuscript. A.V.M. and R.S.M. performed metabolic flux analysis experiments and assisted with in vivo experiments. R.D.W. performed experiments relating to Treg cell function. R.E.D. performed experiments related to Akt function. S.C.W. performed electron microscopy. R.L.F. provided human HNSCC patient PBL and TIL. G.M.D. performed and oversaw research, designed experiments, and wrote the manuscript.

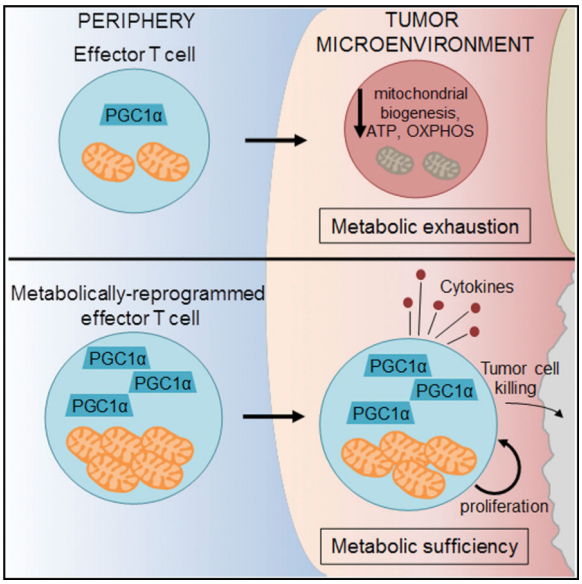

INTRODUCTION

The immune system has evolved multiple cellular mechanisms for the detection and elimination of abnormal or stressed cells in a wide array of environments. Early detection of cancer, via immunosurveillance, can occur almost anywhere, facilitating destruction of early transformed cells expressing neoantigens. However, as cancers edit and escape this initial immune detection, they also generate an immunosuppressive microenvironment which restricts T cell infiltration, activation, and effector function both through direct repression (via cytokines, adenosine, prostaglandins, glucose restriction, etc.) as well as the recruitment of immunosuppressive populations tasked with maintaining immune tolerance (Jiang et al., 2015). The result is an ineffectual antitumor immune response and consequent tumor progression.

Recent advances in cancer immunotherapy have revealed that the T cell response to cancer can be reinvigorated in a variety of ways, resulting in durable and effective benefit in a wide array of cancer types (La-Beck et al., 2015; Mahoney et al., 2015; Ribas, 2015). These include engineering chimeric antigen receptors redirect T cells to tumors, personalized antigen vaccines to persistent neoepitopes, and, probably most prominently, antibody-mediated blockade of co-inhibitory “checkpoint” molecules, like programmed death-1 (PD-1), cytotoxic T lymphocyte antigen 4 (CTLA-4), lymphocyte activation gene 3 (LAG-3), T cell immunoglobulin and mucin-containing gene 3 (Tim-3), among others (La-Beck et al., 2015). These molecules are highly upregulated on tumor-infiltrating T cells and are thought to negatively regulate T cell activation and effector function. This elevated and sustained expression of co-inhibitory molecules is indicative of a hyporesponsive phenotype, originally discovered in chronic viral infection, termed T cell exhaustion (Wherry and Kurachi, 2015). Antigen persistence results in continued TCR and cytokine signals, which promote upregulation of these receptors, resulting in a hyporesponsiveness functionally similar to anergy but mechanistically distinct (Crespo et al., 2013; Schietinger and

Greenberg, 2014). Importantly, T cells can still have an exhausted phenotype in the absence of co-inhibitory molecules (Legat et al., 2013; Odorizzi et al., 2015), shedding light on the fact that while these co-inhibitory molecules have been extensively studied at the molecular and biochemical levels, it is still unclear what the contribution of co-inhibitory molecule signaling is to the initiation or maintenance of the exhausted phenotype. Thus for improving the treatment of cancer, chronic viral infections, and other diseases, it is critical to understand the mechanisms behind the dysfunction in chronically activated T cells (Pauken and Wherry, 2015). This is especially important considering that, while checkpoint blockade has had remarkable success in the clinic, the majority of patients still do not respond to these therapies (La-Beck et al., 2015).

Carrying out effector function is a metabolically demanding process (Pearce et al., 2013). T cells must efficiently divide and replicate their genome rapidly and with fidelity, synthesize high levels of cytokines, and deliver cytotoxic payload to target cells. Recent discoveries of T cells' dependence on nutrient sensing and flux through various metabolic pathways have shown that metabolism represents a key mechanism by which the immune system can be regulated (Delgoffe and Powell, 2015). They also suggest that the fate and function of T cells are intrinsically tied to their metabolism and that a T cell (like any other cell) requires the machinery to generate bioenergetic intermediates to support proliferation and effector function (Delgoffe and Powell, 2015).

T cells utilize aerobic glycolysis, diverting glucose into lactate fermentation rather than mitochondrial acetyl-CoA oxidation to support their expansion and proliferation during their effector phase (Pearce et al., 2013; Roos and Loos, 1970). The precise contributions of this pathway and its teleology remain the subject of much study, but nevertheless the mitochondria remain an essential component of T cell metabolism. Effector T cells significantly upregulate oxidative activity and memory T cell precursors become increasingly dependent on mitochondria to mediate fatty-acid oxidation over time (van der Windt et al., 2012; van der Windt et al., 2013). Furthermore, the mitochondria remain important organelles for biosynthesis, calcium buffering, and mediating programmed cell death (Rizzuto et al., 2012; Wenner, 2012). Thus, while T cells might divert glucose metabolism away from mitochondrial pathways during activation, mitochondria are still critical for maintaining the health and integrity of the T cell in both effector and memory phases.

While the effects of glucose deprivation in tumor microenvironments on glycolytic metabolism and T cell function have garnered much recent interest, the mitochondrial phenotype of T cells infiltrating tumors remains unclear (Chang et al., 2015; Ho et al., 2015; Siska and Rathmell, 2015; Zhao et al., 2015). We have observed that tumor-infiltrating T cells display an overall phenotype of metabolic insufficiency, characterized most prominently by a persistent loss of mitochondrial function and mass. Loss of mitochondrial function in tumor-reactive T cells occurred specifically in the tumor microenvironment, largely independently of PD-1 blockade or regulatory T cell suppression, and due to a defect in PPAR-gamma coactivator 1α (PGC1α)-programmed mitochondrial biogenesis. This defect was due in part to chronic protein kinase B (Akt) signaling, inhibited Foxo transcription factor activity, and consequent PGC1α repression. Metabolic reprogramming

of T cells through enforced PGC1α expression rescued mitochondrial function and induced superior antitumor responses characterized by cytokine production and tumor control. These findings show the chronic activation associated with the anti-cancer response represses oxidative metabolism, suggesting that the dysfunction of tumor-infiltrating T cells might be linked to an ability to generate sufficient metabolic intermediates for cellular function.

RESULTS

Tumor-Infiltrating T Cells Display Decreased Mitochondrial Mass

To assay the metabolic capacity of tumor-infiltrating T cells, we measured mitochondrial function and mass by flow cytometry using MitoTracker Deep Red FM (a membrane permeable, carbocyanine-based dye for mitochondria used previously to stain mitochondrial mass; Cottet-Rousselle et al., 2011) and competency for glucose uptake using fluorescent 2-NBD-glucose (2NBDG) in T cells infiltrating implantable tumors. While Mito-Tracker Deep Red has been shown to be membrane potential sensitive in some systems, uncoupling using carbonyl cyanide m-chlorophenyl hydrazine (CCCP) showed that, using our staining protocols, MitoTracker Deep Red was highly resistant to collapse of membrane potential, especially compared to tetra-methylrhodamine ester (TMRE), a well-known membrane-potential sensitive dye (Figure S1A). C57/BL6 mice were inoculated with B16 melanoma, and at day 12, lymph node and tumor preparations were pulsed with 2-NBDG and stained for flow cytometric analysis. Whereas T cells in the lymph nodes, both non-draining (ndLN) and tumor draining (dLN), effectively took up glucose and had relatively high MitoTracker FM staining, $CD8^+$ tumor infiltrating lymphocytes (TILs) showed a dramatic reduction of mitochondrial mass as well as the ability to take up glucose (Figures 1A and 1B). To confirm the phenotype we were observing was due to loss of mitochondrial mass and not only mitochondrial depolarization, we employed both Mito-Tracker Green FM (another carbocyanine-based dye) and antibodies to the mitochondrial outer membrane protein Voltage Dependent Anion Channel (VDAC), revealing similar losses (Figure S1B). T cells of various effector and memory phenotypes have been shown to have distinct mitochondrial masses (van der Windt et al., 2013), which we confirmed with our dyes; however, these differences are substantially smaller than those observed within the tumor microenvironment (Figure S1C). For clarity, throughout this study we primarily gate solely on $CD8^+$ T cells and without further subdivision unless explicitly stated. This insufficiency was largely specific to $CD8^+$ T cells, as $CD4^+$ T cells retained most of their mitochondrial mass in B16 tumors. This phenotype was common to three different implantable tumor models inoculated into B6 mice, including MC38 adenocarcinoma and Lewis Lung Carcinoma (LLC), with some notable differences. We also observe loss of MitoTracker FM staining in a proportion of $CD4^+$ T cells in LLC, and no significant differences in glucose uptake (Figure 1B and Figures S1D and S1E). This loss of mitochondrial mass was confirmed by transmission electron microscopy, which revealed that tumor-infiltrating $CD8^+$ T cells not only showed lower mitochondrial mass, but also abnormal mitochondrial morphology (Figure 1C). We also examined metabolism in T cells infiltrating human head and neck squamous cell carcinoma (HNSCC) and found a similar loss of mitochondrial staining when compared to peripheral blood T cells (Figure 1D).

We next examined the metabolic output of tumor-infiltrating T cells using a Seahorse extracellular flux analyzer. Metabolic flux analysis of effector, LN-resident, or tumor-infiltrating $CD8^+$ T cells confirmed a defect in oxygen consumption (OCR), with substantial loss of spare respiratory capacity (a measure of mitochondrial reserve, measured as the difference between basal and uncoupled maximal oxygen consumption) compared to naive, LN-resident cells, or previously activated effector T cells (Figure 1E). This resulted in an increased dependence on glycolytic metabolism, as evidenced by increased extracellular acidification rate (Figure 1E). Thus, T cells infiltrating mouse and human tumors showed a loss of mitochondrial mass and dependence of glycolytic metabolism, rendering them unable to carry out critical cellular functions in the glucose-poor tumor microenvironment.

Loss of Mitochondrial Function Is Specific T Cell Responses in the Tumor Microenvironment

We next wanted to determine whether this mitochondrial dysfunction was specific to the anti-tumor response or if it occurred in other types of robust effector responses. To do this, we utilized an adoptive transfer system of naive, congenically mismatched ovalbumin (OVA)-specific TCR transgenic (OT-I) T cells into mice bearing OVA-expressing B16 ($B16^{OVA}$) tumors or mice infected with OVA-expressing *Vaccinia* virus (VV^{OVA}) for 6 days. This experiment was designed to compare the chronic activation seen in cancer to a robust acute in vivo response in which antigen is effectively cleared (Pollizzi et al., 2015). Consistent with our data generated in polyclonal populations from mouse and human tumors, OT-I T cells infiltrating tumors showed decreased MitoTracker FM staining relative to their LN-resident counterparts (Figure 2A, B). In contrast, OT-I T cells responding in the spleen to VV^{OVA} infection had increased mitochondrial mass compared to splenic OT-I T cells adoptively transferred into mock infected mice, as evidenced by increased MitoTracker FM and intracellular VDAC staining (Figure 2A, Figure S2A). T cells responding to OVA in the context of VV^{OVA} also increased basal oxygen consumption (OCR) and spare respiratory capacity (Figure 2B). VV^{OVA}-responsive T cells also displayed heightened glycolytic function, even compared to OT-I T cells isolated from tumors (Figure 2B). Comparisons of ATP reserves from OT-I T cells responding in $B16^{OVA}$ tumors compared to VV^{OVA}-infected spleens revealed that TILs showed an inability to maintain ATP reserves, while this pool was dramatically increased in cells responding to viral infection (Figure 2C). Functionally this led to differential patterns of cytokine production upon peptide or phorbol 12-myristate 13-acetate/ionomycin re-stimulation (Figure S2B). The phenotype of mitochondrial insufficiency observed in tumor-infiltrating lymphocytes was quite stable; OT-I T cells isolated from $B16^{OVA}$ tumors retained a phenotype of low mitochondrial mass, even when isolated and transferred into a new, VV^{OVA} infected mouse for 7 days (Figure 2D). Thus, T cell dysfunction associated with loss of mitochondria occurred specifically within the chronic activation and microenvironment of cancer.

Mitochondria Become Dysfunctional as T Cells Are Activated in Tumors

We next utilized this adoptive transfer model to explore the metabolic consequences of activated T cells as they enter the tumor microenvironment versus responding to acute infection. Naive, OT-I $Thy1.1^+$ T cells were labeled with CellTrace Violet (CTV) to monitor proliferation and transferred into $B16^{OVA}$-bearing or VV^{OVA}-infected C57BL/6 ($Thy1.2^+$)

mice for 72 hr. This resulted in robust proliferation in both scenarios, with OT-I T cells undergoing as many as seven cell divisions (Figure 3A). We also observed loss of mitochondrial mass as T cells enter the tumor microenvironment, just as we had shown with longer incubations (6 days, Figure 2A). Experiments employing dichlorofluorescin diacetate (DCFDA), a reactive oxygen species (ROS) indicator, and TMRE, a mitochondrial membrane potential-sensitive dye (Figure S1A), indicated that T cells responding to antigen in the tumor microenvironment showed mitochondrial depolarization as well as a loss of ROS production (Figures 3B and 3C). Because mitochondrial depolarization can lead to autophagy, we then asked whether mitophagy may be mediating the loss of mitochondria in tumor-infiltrating T cells. We did not observe any significant increases in Light Chain 3B (LC3B) staining in permeabilized OT-I T cells, suggesting that autophagic processes are likely not overtly deregulated in these cells (Figure 3D). We also treated tumor-bearing mice 24 hr after transfer with the mitophagy and mitochondrial fission inhibitor m-divi-1 (Cui et al., 2010); this also failed to improve mitochondrial staining in tumor infiltrating T cells (Figure 3E). We also asked whether loss of mitochondrial function could occur in vitro in response to co-culture with tumor cells, and found that response of naive or previously activated OT-I T cells to $B16^{OVA}$ tumor cells in vitro did not result in mitochondrial loss (Figures S3A and S3B). Thus, T cells responding to cancer lost oxidative metabolism relatively rapidly, but this required signals that are present specifically in the tumor microenvironment.

Loss of Mitochondrial Mass Correlates with Upregulation of Co-inhibitory Molecules

As loss of mitochondrial function was progressive and specific to the tumor microenvironment, we next sought to determine the relationship between the loss of mitochondria seen in tumor-infiltrating T cells and the expression of molecular markers for dysfunctional, exhausted T cells. B16 melanoma is highly enriched for dysfunctional T cells expressing high levels of PD-1, LAG-3, and Tim-3 (Figure 4A). Mitochondrial loss in the polyclonal T cell response appeared to be progressive, as T cells expressing more co-inhibitory molecules had decreased mitochondrial mass, as evidenced by MitoTracker FM staining as well as staining for VDAC (Figures 4B, 4C, and S4A). Whereas mitochondrial mass was inversely correlated with upregulation of coinhibitory molecules, glucose competency was consistently depressed in tumor-infiltrating T cells and did not specifically correlate with these markers (Figure 4D), in agreement with previous reports (Chang et al., 2015; Ho et al., 2015). This resulted in a failure to maintain a sufficient reserve of ATP (as measured directly ex vivo) (Figure 4E). We observed similar results in MC38 and LLC tumors (Figure S4B and S4C). LLC did not induce similar sustained co-inhibitory molecule expression in $CD8^+$ T cells (compared to the other two models) (Figure S4C) but still exhibited a significant mitochondrial defect (Figures 1B and S1). $CD8^+$ T cells infiltrating head-and-neck cancers exhibited decreased MitoTracker staining compared to peripheral blood lymphocyte T cells (Figure 1D) and high levels of coinhibitory molecule expression (Figure 4F) that correlated with mitochondrial loss (Figure 4G). In order to determine whether, directly, lower MitoTracker FM staining correlated with poor cytokine production, we sorted tumor-infiltrating T cells based on MitoTracker FM staining and stimulated them 16 hr to monitor cytokine production. Consistent with their exhausted phenotype, T cells having lowest mitochondrial staining had the lowest cytokine production (Figure S4D).

Thus, T cells infiltrating solid tumors showed a progressive loss of mitochondrial mass and function, such that the most exhausted cells show the lowest mitochondrial activity.

Loss of T Cell Oxidative Metabolism in Cancer Is Largely Independent of PD-1 Signaling and Treg Cells

PD-1 blockade can reverse tumor-induced T cell dysfunction and lead to heightened antitumor immunity and cancer regression (La-Beck et al., 2015). We thus wanted to determine whether PD-1 blockade might rescue loss of mitochondrial function in tumor-infiltrating T cells. We employed mice bearing B16 tumors, in which PD-1 therapy is ineffective, despite the presence of large numbers of PD-1^+ T cells, as well as those bearing MC38 tumors, which is sensitive to PD-1 monotherapy (Woo et al., 2012). Mice were inoculated with B16 or MC38 and received anti-PD-1 (200 μg, thrice weekly) or its isotype control when palpable tumors were present (1 × 1 mm). Regardless of treatment or tumor type, tumor-infiltrating T cells showed similar decreases in mitochondrial mass (Figures 5A and 5B). Our PD-1 blockade strategy was therapeutically effective, resulting in 40% regression in MC38 bearing mice (Figure 5C). In order to determine whether PD-1 signaling might impact the mitochondrial sufficiency of recent entrants into the tumor, we transferred dye-labeled OT-I T cells into mice bearing established $B16^{OVA}$ tumors under the cover of PD-1 blockade or its control for 72 hr. We could observe a temporary and incomplete recovery of MitoTracker FM staining in later cell divisions (Figure 5D). However, these changes were statistically significant only when analyzed as broken down by cell division and could not be sustained or detected past 72 hr (data not shown). Thus, although PD-1 might play a role in modulation of metabolism, blockade of PD-1 was not sufficient to reverse mitochondrial insufficiency observed in tumor-infiltrating T cells.

Regulatory T cells (Treg) also represent a major immunosuppressive player in the tumor microenvironment (Liu et al., 2016). Thus, we asked whether Treg cells mediate metabolic insufficiency in the tumor microenvironment by examining $CD8^+$ TILs from *Foxp3*$^{DTR.GFP}$ mice which carry a diphtheria toxin receptor and green fluorescent protein (GFP) knocked into the 3′ UTR of *Foxp3*, allowing for conditional deletion of Treg cells upon treatment with diphtheria toxin (DT) (Kim et al., 2007a). Treatment of B16-bearing *Foxp3*$^{DTR.GFP}$ mice with DT resulted in near complete depletion of tumor-infiltrating Treg cells (Figure S5A) but no significant increases in $CD8^+$ T cell MitoTracker FM staining (Figure S5B). In agreement with these in vivo findings, $CD8^+$ T cells suppressed in vitro by purified Treg cells also maintained mitochondrial sufficiency (Figure S5C). Thus, metabolic insufficiency in $CD8^+$ TILs appeared to be driven in a manner independent of “classic” immunosuppressive mechanisms in the tumor microenvironment.

PGC1α-Mediated Mitochondrial Biogenesis Is Repressed by Akt in Tumor-Infiltrating T Cells

Having found that PD-1 and Treg cells did not appear to outright cause the mitochondrial dysfunction seen in tumor-infiltrating T cells, we next sought to determine the molecular mechanism for this metabolic phenotype. Our kinetic analyses showed that these T cells divided extremely rapidly in response to tumor antigen in the LNs, so we hypothesized that T cells failed to properly program mitochondrial biogenesis during rapid cell division upon

entry into the tumor microenvironment. Mitochondrial replication is programmed in part by the mitochondrial transcription factor A (TFAM) and regulated by the transcriptional coactivator PGC1α (encoded by *Ppargc1a*) (Finck and Kelly, 2006; Spiegelman, 2007). Intracellular staining and quantitative PCR analysis revealed tumor infiltrating $CD8^+$ T cells exhibit decreased PGC1α protein and *Ppargc1a* expression, respectively (Figure 6A and Figure S6A). Kinetic analysis of dye labeled, naive OT-I cells injected into $B16^{OVA}$-bearing mice showed PGC1α downregulation occurred concomitant with cell division specifically in the tumor microenvironment, suggesting microenvironment-derived signals promoted downregulation of mitochondrial biogenesis during T cell proliferation (Figure 6B). Repression of PGC1α occurred even in the presence of PD-1 blockade, suggesting another dominant signal present in the tumor microenvironment suppresses PGC1α expression (Figure S6B). Analysis of PGC1α-deficient T cells (*Ppargc1a*$^{f/f}$*Cd4*^{Cre} mice) revealed progressive losses of mitochondrial mass in vitro after activation, resulting in decreased OCR (Figures S6C and S6D). Comparison of cytokine production in LN- and TIL OT-I T cells responding to cognate peptide revealed that the small proportion of $PGC1\alpha^+$ cells in tumor-infiltrating compartments marked the T cells that were competent to produce cytokines, indicating that this pathway is important for intratumoral T cell function (Figure 6C). In agreement with this observation, T cells showing repressed PGC1α staining also exhibited decreased T-bet and Ki-67 staining, consistent with a model in which PGC1α repression is concomitant with a terminally exhausted phenotype (Figures S6E and S6F).

PGC1α is dynamically regulated by a number of signaling pathways relevant to T cell activation, but a prominent repressive pathway is mediated by Akt (Fernandez-Marcos and Auwerx, 2011). Akt has been shown to upregulate glycolytic metabolism through a variety of mechanisms, but it also can actively repressive oxidative programs, particularly through the phosphorylation and consequent inactivation of Foxo family transcription factors, shown previously to promote PGC1α expression (Borniquel et al., 2010; Olmos et al., 2009). Thus, we sought to examine the Akt status of tumor-infiltrating T cells, hypothesizing that the chronic activation signals mediated by persistent antigen in cancer might promote Akt activation and repress the oxidative phenotype programmed by Foxo. $CD8^+$ T cells infiltrating B16 tumors show increased Akt activation (as measured by phosphorylation at serine 473) and Akt-mediated inhibitory Foxo phosphorylation compared to LN (where the vast majority of T cells are resting) (Figure 6D). Comparison of Akt activation to PD-1 status revealed that Akt is highest in tumor-infiltrating T cells that are PD-1^{mid} as well as those having high PD-1 and LAG-3 surface expression, suggesting that Akt is persistent in newly activated T cells as well as those receiving chronic stimulation and differentiating toward terminal exhaustion (Figure S6G). Importantly, intratumoral cells that have high degrees of Akt activation are particularly low in PGC1α protein levels (Figures 6E). We also examined early (3 day) and late (6 day) responses of T cells responding to $B16^{OVA}$ or VV^{OVA}, and found that while Akt activation in acute viral infection was transient, T cells activated in the tumor microenvironment appeared to show chronic Akt signaling, persisting 6 days after adoptive transfer (Figure 6F) Short-term treatment (72 hr) of B16-bearing mice with a potent Akt kinase inhibitor revealed the Akt, in part, mediated losses in PGC1α and mitochondrial sufficiency, such that treatment with Akt inhibitor resulted in partial rescue of the metabolically suppressed phenotype (Figures 6G and 6H). Thus, T cells responding in

tumor microenvironments repressed mitochondrial biogenesis through repression of PGC1α, driven, in part, by chronic Akt activation and consequent repression of Foxo activity.

Metabolic Reprogramming of Tumor-Specific T Cells Results in Increased Antitumor Immunity

Having demonstrated that PGC1α acted as a node of dysregulation for mitochondrial sufficiency in tumor-specific T cells, we thus wondered whether reprogramming T cells to favor mitochondrial biogenesis would result in increased intratumoral T cell persistence and function. To this end, we generated retro-viral vectors to overexpress PGC1α and transduced OT-I T cells. PGC1α overexpression significantly increased mitochondrial mass early (48 and 96 hr) after transduction in in vitro culture, although during the expansion phase, empty-vector expressing cells initiate mitochondrial biogenesis and eventually reach equivalency to their reprogrammed counterparts (Figure 7A). However, even at this later stage, PGC1α-reprogrammed T cells showed significantly increased OXPHOS (Figure 7A). PGC1α-overexpressing T cells exhibited upregulation of spare respiratory capacity (Figure 7A), indicating high mitochondrial reserve and that mitochondrial biogenesis was primed in these reprogrammed cells. We did not observe any significant increases in aerobic glycolysis (ECAR), although we did observe a trend in some experiments (Figure 7A). We then determined whether any particular carbon source dominated this increase in SRC. FCCP-uncoupled T cells were treated with inhibitors of pyruvate, fatty acid, or glutamine oxidation, revealing that the increased respiratory capacity did not preferentially apply to a particular carbon source, suggesting that mitochondrial capacity was improved generally when PGC1α expression was enforced (Figure S7A). In vitro, these T cells exhibited similar effector function as their control counterparts, suggesting that in this environment where nutrients are not limiting, T cells are operating more or less at maximal capacity (Figure S7B). OT-I T cells overexpressing PGC1α transferred into mice with established $B16^{OVA}$ tumors were resistant to loss of mitochondrial sufficiency and highly enriched in the tumor microenvironment (Figure 7B). Restimulation with OVA peptide showed that these metabolically reprogrammed T cells were superior at producing type 1 cytokines, compared to their wild-type counterparts (Figure 7C). Notably, these reprogrammed T cells expressed (at even higher levels than EV) co-inhibitory molecules, suggesting retention of mitochondrial function promoted further activation and upregulation of these checkpoint molecules (Figure S7C). Having found that PGC1α-reprogrammed T cells displayed increased effector function, we then tested whether these T cells had better therapeutic efficacy. Mice bearing small (2–6 mm^2) $B16^{OVA}$ tumors received an adoptive transfer of 250,000 (if tumor was < 4 mm^2) or 500,000 (if starting tumor was > 4 mm^2) PGC1α or empty-vector transduced OT-I T cells, and tumor growth was measured over time. PGC1α-reprogrammed T cells showed enhanced antitumor efficacy resulting in significantly prolonged survival and higher incidence of complete regressions (20%) in this aggressive tumor model (Figures 7D and 7E). Thus, reprogramming tumor-specific T cells to favor mitochondrial biogenesis protected them from the loss of function observed in the tumor microenvironment.

DISCUSSION

Our data place persistence and function of mitochondria as central to sustained effector function of T cells, especially those under continual stimulation as in cancer or chronic viral infections. Observed most prominently in $CD8^+$ T cells specifically in the tumor microenvironment, we observed progressive and persistent loss of mitochondrial function and mass. At least in the time course of rapidly growing tumor, this effect could be observed concomitantly with PD-1 upregulation but largely independently of treatment with anti-PD-1, with only mild and temporary increases observed in response to blockade of this particular checkpoint. Rather, Akt signaling, associated with chronic activation, resulted in repression of oxidative metabolism, thus driving an unsustainable metabolic program. Our data bring to light the metabolic nature of T cell dysfunction, in cancer and in general.

While glucose metabolism, especially aerobic glycolysis, has been heavily studied as a key mediator of T cell effector fate and function, our study suggests that mitochondrial function and mass are dynamically regulated and required to maintain optimal effector function. This is consistent with data recently generated suggesting mitochondrial membrane potential may predict stemness in tumor-infiltrating T cells, and that cytokine production might be increased in T cells that display high mitochondrial activity (Sukumar et al., 2016).

As mentioned previously, there is some debate whether Mito-Tracker Deep Red FM is a potentiometric dye or one that stains for mitochondrial mass irrespective of membrane potential (Xiao et al., 2016). Our data employing uncoupling agents such as CCCP indicated that although Deep Red FM might show some sensitivity for membrane potential at high doses, this paled in comparison to results with TMRE, a true potentiometric dye. We believe our corollary data employing MitoTracker Green and VDAC antibodies indeed confirm that T cells infiltrating tumors exhibit losses of mitochondrial function and total mass, consistent with repressed PGC1α-mediated mitochondrial biogenesis. Whereas effector T cells have been shown to possess fewer mitochondria than their memory counterparts (van der Windt et al., 2012; van der Windt et al., 2013), it is unclear how chronic stimulation might alter this fate. Our data suggest that the continued, inflammatory activation of T cells in cancer promotes a defect in mitochondrial biogenesis, mediated in part by Akt-controlled inhibition of Foxo-programmed PGC1α transcription. While Akt does repress oxidative metabolism, more traditional roles for Akt suggest its potential as an in vivo therapeutic target might be limited, because T cells might require Akt and downstream signaling in situ to mediate effector functions (Macintyre et al., 2011). However, recent studies have revealed that this might not be the case. Akt inhibition has been employed in preclinical and translational settings as a means to reinvigorate TIL expansion, in part through modulating oxidative metabolism (Crompton et al., 2015). In addition, T cells lacking the mammalian target of rapamycin complex 2, the kinase for the hydrophobic motif (serine 473, measured in this study) of Akt, show superior effector function and increased oxidative metabolism, suggesting full Akt activation might not be acutely required for effector function (Pollizzi et al., 2015). Thus, our data identify PGC1α as a crucial mechanistic link between Akt and repressed oxidative metabolism in tumor-infiltrating T cells. In addition, Akt inhibitors, which are currently being evaluated in clinical trials as anti-cancer agents, might have immunomodulatory effects that could synergize with immunotherapies.

PD-1 has been shown to inhibit mammalian target of rapamycin complex 1 signaling (which has metabolic consequences), as well as modulating metabolism at the genetic level (Wherry and Kurachi, 2015). However, we only observed association between PD-1 upregulation and mitochondrial insufficiency, with mild and short-lived effects on mitochondrial metabolism arising from anti-PD-1 treatment. In the tumor, there might be too many other signals to be offset by PD-1 blockade alone or other co-inhibitory molecules like LAG-3 or TIGIT might be playing additional roles in modulating lymphocyte metabolism. Likewise, we failed to see any effect of regulatory T cell suppression on mitochondrial function and mass, both using a genetic model of Treg cell depletion, *Foxp3*$^{DTR.GFP}$ mice treated with diphtheria toxin in established tumors, as well as coculture of purified Treg cells with activated CD8^{+} T cells.

Our data point to PGC1α as a key node of signal integration tying a diverse array of cellular signals (including Akt signaling) to mitochondrial biogenesis. Type I and type II interferons, tumor necrosis factor, interleukin-12, energy charge, and low NAD^{+}/NADH or oleate/palmitate ratios have been shown to repress PGC1α expression, localization or transcriptional activity through a variety of signaling pathways (Alvarez-Guardia et al., 2010; Haghikia et al., 2015; Kauppinen et al., 2013; Kim et al., 2007b; Palomer et al., 2009; Scarpulla, 2011). PGC1α is post-translationally modified by a number of signaling pathways important in T cell biology (Akt, p38-MAPK, AMPK, SIRT1, PRMT1) (Fernandez-Marcos and Auwerx, 2011). Thus, the balance of these signals in the inflammatory milieu might determine PGC1α activity and its ability to program mitochondrial biogenesis.

This study adds to a growing number of reports that collectively suggest that the T cell exhaustion observed in chronic activation has underpinnings in basic cellular processes like metabolism. Unlike anergy (induced by minimal signaling, TCR ligation alone, in a non-inflammatory environment), persistent, inflammatory activation in cancer and chronic viral infections promote an effector state that T cells cannot sustain (Jiang et al., 2015; Schietinger and Greenberg, 2014; Wherry and Kurachi, 2015). This is especially perilous in the tumor microenvironment, because chronic inflammatory signals might drive a sustained reliance on glycolysis in a tissue site where glucose levels are extremely low (Siska and Rathmell, 2015). We and others reveal that T cells show depressed glucose uptake compared to LN-resident cells and glycolysis compared to matched, virus-activated cells, suggesting that, generally, T cell exhaustion is characterized by metabolic insufficiency (Chang et al., 2015; Ho et al., 2015; Zhao et al., 2015). Teleologically, T cells in metabolic distress might upregulate co-inhibitory molecules as a means to prevent terminal loss of metabolic sufficiency or survival, a model consistent with results obtained in chronic viral infection (Staron et al., 2014). These metabolic defects can be persistent even when removed from that microenvironment which might provide a potential explanation for situations in which concomitant tumor immunity is lost at distal sites.

Finally, our data strongly support modulation and reprogramming of the metabolic state as a strategy for the improvement of immunotherapy for cancer. While advances in checkpoint blockade and other types of immunotherapy have revealed that the mechanisms blocking immune cell activation can be altered by therapeutic intervention, tumors present a harsh

microenvironment that is immunosuppressive by its basic nature. Further, our data suggest that the metabolic status of individual tumor microenvironments and their respective T cell infiltrates, which can vary from model to model or, more importantly, patient to patient, might help predict the response to immunotherapies like checkpoint blockade. While our study demonstrates that the direct metabolic reprogramming of T cells can have efficacy, it might be advantageous to adopt other strategies to remodel the metabolism of the microenvironment itself in order to create a more permissive environment for T cell activity.

Metabolism is central to cellular function, so it is largely unsurprising that T cells fail in nutrient-poor conditions. Our results and others' have shed light on the fact that during chronic activation, as in cancer, T cells are driven to proliferate and perform effector function at the expense of their continued persistence and longevity. Development of strategies to modify the bioenergetics of T cells or the tumor microenvironment itself has the promise to improve and synergize with other forms of immunotherapy to increase the efficacy of the treatment of cancer.

EXPERIMENTAL PROCEDURES

Mice

Animal work was done in accordance with the Institutional Animal Care and Use Committee of the University of Pittsburgh. All mice were housed in specific pathogen free conditions prior to use. C57/BL6, SJ/L (Thy1.1), *Ppargc1a*$^{f/f}$, *Cd4*^{Cre}, *Foxp3*$^{GFP.Cre.ERT2}$, *Foxp3*$^{DTR.GFP}$, and OT-I mice were obtained from The Jackson Laboratory.

Cell Lines, Antibodies, and Other Reagents

B16-F10 and LLC were obtained from ATCC. MC38 was obtained from Dario Vignali. B16^{OVA} (MO5) was obtained from Per Basse and Lou Falo. OVA-ex-pressing *Vaccinia* virus was originally generated by Yewdell and Bennink and obtained from Jonathan Powell. Most antibodies for flow cytometry were obtained from BioLegend. MitoTracker Green FM, MitoTracker Deep Red FM, tetramethylrhodamine ester (TMRE), and H2-DCFDA were obtained from ThermoFisher. VDAC antibody was obtained from Abcam. LC3B, pAktS473, pFoxo1/3a antibodies were obtained from Cell Signaling Technologies and detected after surface staining with simultaneous fixation and permabilization in 1.5% PFA madeup in 1X Permeabilization buffer (eBioscience). 2-NBD-glucose, m-divi-1, and Akt inhibitor VIII were purchased from Cayman Chemical. PGC1α antibody (H-300) was obtained from Santa Cruz Biotechnology, and was detected using the Foxp3 Fix/Perm kit (eBioscience) and Alexa Fluor 647 or Alexa Fluor 488-conjugated anti-rabbit immunoglobulin G (IgG) (Jackson Immunoresearch). Anti-PD-1 blocking antibody (J43) and its hamster IgG control were obtained from Bio-X-Cell. CellTrace Violet was purchased from eBioscience, and CFSE was purchased from BioLegend.

T Cell Isolations from Lymph Node and Tumor and Adoptive Transfer

Spleen and lymph node CD8$^+$ T cells were isolated from 6- to 8-week-old OT-I (Thy1.2 or Thy1.1) mice. Tissue was harvested, mechanically disrupted, and incubated with a biotinylated antibody cocktail consisting of antibodies (BioLegend) to B220, CD11b,

CD11c, CD16/32, CD19, CD25, CD105, NK1.1,TCRγδ, and CD4. After a wash step, cells were incubated with streptavidin-coated magnetic nanoparticles (BioLegend). After washing, $CD8^+$ cells were isolated by applying a magnetic field and removing untouched cells. These OT-I $CD8^+$ T cells were also labeled with the proliferation dye CellTrace Violet according to the manufacturer's protocol. Mice bearing $B16^{OVA}$ tumors or immunized with VV^{OVA} received cells intravenously. To obtain single-cell suspensions of tumor infiltrating lymphocytes, excised, we injected whole tumors repeatedly using 20G needles with 2 mg/mL collagenase type VI, 2 U/mL hyluronidase (Dispase), and 10 U/mL DNase I (Sigma) in buffered RPMI with 10% FBS and incubated them for 30 min at 37°C. Tumors were mechanically disrupted between frosted glass slides and filtered to remove particulates, then vortexed for 2 min. In many experiments (especially prior to sorting), tumor homogenates were debulked of tumor cells using CD105-biotin mediated magnetic depletion.

Human Peripheral Blood Lymphocyte or Tumor Infiltrating Lymphocyte Isolation

After approval by Institutional Review Board (University of Pittsburgh Cancer Institute (UPCI) protocol 99-069], informed consent was obtained from each patientt before blood withdrawal. Blood from patients with HNC treated with cetuximab during or within 1 month of treatment (UPCI clinical trial #08-013 NCT 01218048). Fresh tumors from patients with HNC were minced into small pieces manually, transferred to 70 μm cell strainers (BD), and mechanically separated using the plunger of a 5 ml syringe. Lymphocytes were purified by Ficoll-Paque PLUS centrifugation following standard protocol (Amersham Biosciences), pulsed with 2NBDG, and stained for flow cytometry.

Metabolism Assays

Nondraining and draining lymph node or tumor preparations were pulsed with 20 μM 2-NBDG (Cayman Chemical) in 5% FBS-containing media for 30 min at 37°C. Cells were surface stained and loaded with MitoTracker FM (ThermoFisher) dyes or TMRE to measure mitochondrial mass and function.

T cells were plated on Cell-Tak coated Seahorse culture plates (50,000 or 100,000 T cells/well) in assay media consisting of minimal, unbuffered DMEM supplemented with 1% BSA and 25 mM glucose, 1 μM pyruvate, and 2 mM glutamine and analyzed using a Seahorse XFe96 (Agilent). Basal extracellular acidification and oxygen consumption rates were taken for 30 min. Cells were stimulated with oligomycin (2 μM), FCCP (0.5 μM), 2-deoxyglucose (100mM) and rotenone/antimycin A (100 μM) to obtain maximal respiratory and control values. Spare respiratory capacity is measured as the difference between basal OCR values and maximal OCR values obtained after FCCP uncoupling.

Electron Microscopy

$CD8^+$ T cells were sorted from LNs and TIL and fixed in 4% glutaraldehyde and stained for electron microscopy as previously described. (Li et al., 2013)

Retroviral Expression

PGC1α was originally generated by B. Spiegelman, obtained from Addgene (plasmid 1026) (Monsalve et al., 2000), and cloned into an MSCV-driven retroviral expression vector which

also encodes an IRES-mCherry cassette, from Dario Vignali. This vector was transiently transfected into Phoenix ecotropic cells. OT-I splenocytes were stimulated with SIINFEKL peptide at 250 ng/mL in the presence of 100U/mL IL-2 for 24 hr. Retroviral supernatants were harvested, and filtered, and supplemented with 6 μg/mL polybrene. OT-I T cell cultures were spinduced with the retroviral supernatant for 90 min at 2,500 rpm. 24 hr later spinduction this was repeated. Cells were expanded and sorted by mCherry prior to analysis and adoptive transfer.

Supplementary Material

Refer to Web version on PubMed Central for supplementary material.

Acknowledgments

The authors thank Dario Vignali, Larry Kane, and Jonathan Powell for critical reading and comments on this manuscript. We also thank the UPCI Flow Cytometry (especially E. Michael Meyer and Batta Janjic), Cell and Tissue Imaging (Mara Sullivan and Donna Beer Stolz), and Animal Facilities (supported by CCSG P30CA047904). This work was supported in part by the Sidney Kimmel Foundation for Cancer Research (SKF-015-039 to G.M.D.) and the NIH (1S10OD016236-01 to S.C.W., P50 CA097190 Head and Neck Cancer SPORE to R.L.F., and P50CA121973 Skin Cancer SPORE [developmental research award] to G.M.D.).

REFERENCES

Alvarez-Guardia D, Palomer X, Coll T, Davidson MM, Chan TO, Feldman AM, Laguna JC, Vázquez-Carrera M. The p65 subunit of NF-kappaB binds to PGC-1alpha, linking inflammation and metabolic disturbances in cardiac cells. Cardiovasc. Res. 2010; 87:449–458. [PubMed: 20211864]

Borniquel S, García-Quintáns N, Valle I, Olmos Y, Wild B, Martínez-Granero F, Soria E, Lamas S, Monsalve M. Inactivation of Foxo3a and subsequent downregulation of PGC-1 alpha mediate nitric oxide-induced endothelial cell migration. Mol. Cell. Biol. 2010; 30:4035–4044. [PubMed: 20547753]

Chang CH, Qiu J, O'Sullivan D, Buck MD, Noguchi T, Curtis JD, Chen Q, Gindin M, Gubin MM, van der Windt GJ, et al. Metabolic Competition in the Tumor Microenvironment Is a Driver of Cancer Progression. Cell. 2015; 162:1229–1241. [PubMed: 26321679]

Cottet-Rousselle C, Ronot X, Leverve X, Mayol J-F. Cytometric assessment of mitochondria using fluorescent probes. Cytometry A. 2011; 79:405–425. [PubMed: 21595013]

Crespo J, Sun H, Welling TH, Tian Z, Zou W. T cell anergy, exhaustion, senescence, and stemness in the tumor microenvironment. Curr. Opin. Immunol. 2013; 25:214–221. [PubMed: 23298609]

Crompton JG, Sukumar M, Roychoudhuri R, Clever D, Gros A, Eil RL, Tran E, Hanada K, Yu Z, Palmer DC, et al. Akt inhibition enhances expansion of potent tumor-specific lymphocytes with memory cell characteristics. Cancer Res. 2015; 75:296–305. [PubMed: 25432172]

Cui M, Tang X, Christian WV, Yoon Y, Tieu K. Perturbations in mitochondrial dynamics induced by human mutant PINK1 can be rescued by the mitochondrial division inhibitor mdivi-1. J. Biol. Chem. 2010; 285:11740–11752. [PubMed: 20164189]

Delgoffe GM, Powell JD. Feeding an army: The metabolism of T cells in activation, anergy, and exhaustion. Mol. Immunol. 2015; 68(2 Pt C):492–496. [PubMed: 26256793]

Fernandez-Marcos PJ, Auwerx J. Regulation of PGC-1α, a nodal regulator of mitochondrial biogenesis. Am. J. Clin. Nutr. 2011; 93:884S–890S. [PubMed: 21289221]

Finck BN, Kelly DP. PGC-1 coactivators: inducible regulators of energy metabolism in health and disease. J. Clin. Invest. 2006; 116:615–622. [PubMed: 16511594]

Haghikia A, Faissner S, Pappas D, Pula B, Akkad DA, Arning L, Ruhrmann S, Duscha A, Gold R, Baranzini SE, et al. Interferon-beta affects mitochondrial activity in CD4+ lymphocytes: Implications for mechanism of action in multiple sclerosis. Multiple sclerosis (Houndmills, Basingstoke, England). 2015; 21:1262–1270.

Ho PC, Bihuniak JD, Macintyre AN, Staron M, Liu X, Amezquita R, Tsui YC, Cui G, Micevic G, Perales JC, et al. Phosphoenolpyruvate Is a Metabolic Checkpoint of Anti-tumor T Cell Responses. Cell. 2015; 162:1217–1228. [PubMed: 26321681]

Jiang Y, Li Y, Zhu B. T-cell exhaustion in the tumor microenvironment. Cell death & disease. 2015; 6:e1792. [PubMed: 26086965]

Kauppinen A, Suuronen T, Ojala J, Kaarniranta K, Salminen A. Antagonistic crosstalk between NF-κB and SIRT1 in the regulation of inflammation and metabolic disorders. Cell. Signal. 2013; 25:1939–1948. [PubMed: 23770291]

Kim JM, Rasmussen JP, Rudensky AY. Regulatory T cells prevent catastrophic autoimmunity throughout the lifespan of mice. Nat. Immunol. 2007a; 8:191–197. [PubMed: 17136045]

Kim MS, Sweeney TR, Shigenaga JK, Chui LG, Moser A, Grunfeld C, Feingold KR. Tumor necrosis factor and interleukin 1 decrease RXRalpha, PPARalpha, PPARgamma, LXRalpha, and the coactivators SRC-1, PGC-1alpha, and PGC-1beta in liver cells. Metabolism. 2007b; 56:267–279. [PubMed: 17224343]

La-Beck NM, Jean GW, Huynh C, Alzghari SK, Lowe DB. Immune Checkpoint Inhibitors: New Insights and Current Place in Cancer Therapy. Pharmacotherapy. 2015; 35:963–976. [PubMed: 26497482]

Legat A, Speiser DE, Pircher H, Zehn D, Fuertes Marraco SA. Inhibitory Receptor Expression Depends More Dominantly on Differentiation and Activation than “Exhaustion” of Human CD8cT Cells. Front. Immunol. 2013; 4:455. [PubMed: 24391639]

Li HH, Li J, Wasserloos KJ, Wallace C, Sullivan MG, Bauer PM, Stolz DB, Lee JS, Watkins SC, St Croix CM, et al. Caveolae-dependent and -independent uptake of albumin in cultured rodent pulmonary endothelial cells. PLoS ONE. 2013; 8:e81903. [PubMed: 24312378]

Liu C, Workman CJ, Vignali DA. Targeting Regulatory T Cells in Tumors. FEBS J. 2016; 283 Published online March 1, 2016. http://dx.doi.org/10.1111/febs.13656.

Macintyre AN, Finlay D, Preston G, Sinclair LV, Waugh CM, Tamas P, Feijoo C, Okkenhaug K, Cantrell DA. Protein kinase B controls transcriptional programs that direct cytotoxic T cell fate but is dispensable for T cell metabolism. Immunity. 2011; 34:224–236. [PubMed: 21295499]

Mahoney KM, Rennert PD, Freeman GJ. Combination cancer immunotherapy and new immunomodulatory targets. Nat. Rev. Drug Discov. 2015; 14:561–584. [PubMed: 26228759]

Monsalve M, Wu Z, Adelmant G, Puigserver P, Fan M, Spiegelman BM. Direct coupling of transcription and mRNA processing through the thermogenic coactivator PGC-1. Mol. Cell. 2000; 6:307–316. [PubMed: 10983978]

Odorizzi PM, Pauken KE, Paley MA, Sharpe A, Wherry EJ. Genetic absence of PD-1 promotes accumulation of terminally differentiated exhausted CD8+ T cells. J. Exp. Med. 2015; 212:1125–1137. [PubMed: 26034050]

Olmos Y, Valle I, Borniquel S, Tierrez A, Soria E, Lamas S, Monsalve M. Mutual dependence of Foxo3a and PGC-1alpha in the induction of oxidative stress genes. J. Biol. Chem. 2009; 284:14476–14484. [PubMed: 19324885]

Palomer X, Alvarez-Guardia D, Rodríguez-Calvo R, Coll T, Laguna JC, Davidson MM, Chan TO, Feldman AM, Vázquez-Carrera M. TNF-alpha reduces PGC-1alpha expression through NF-kappaB and p38 MAPK leading to increased glucose oxidation in a human cardiac cell model. Cardiovasc. Res. 2009; 81:703–712. [PubMed: 19038972]

Pauken KE, Wherry EJ. Overcoming T cell exhaustion in infection and cancer. Trends Immunol. 2015; 36:265–276. [PubMed: 25797516]

Pearce EL, Poffenberger MC, Chang CH, Jones RG. Fueling immunity: insights into metabolism and lymphocyte function. Science. 2013; 342:1242454. [PubMed: 24115444]

Pollizzi KN, Patel CH, Sun IH, Oh MH, Waickman AT, Wen J, Delgoffe GM, Powell JD. mTORC1 and mTORC2 selectively regulate $CD8^+$ T cell differentiation. J. Clin. Invest. 2015; 125:2090–2108. [PubMed: 25893604]

Ribas A. Adaptive Immune Resistance: How Cancer Protects from Immune Attack. Cancer Discov. 2015; 5:915–919. [PubMed: 26272491]

Rizzuto R, De Stefani D, Raffaello A, Mammucari C. Mitochondria as sensors and regulators of calcium signalling. Nat. Rev. Mol. Cell Biol. 2012; 13:566–578. [PubMed: 22850819]

Roos D, Loos JA. Changes in the carbohydrate metabolism of mitogenically stimulated human peripheral lymphocytes. I. Stimulation by phytohaemagglutinin. Biochim. Biophys. Acta. 1970; 222:565–582. [PubMed: 5496487]

Scarpulla RC. Metabolic control of mitochondrial biogenesis through the PGC-1 family regulatory network. Biochimica et Biophysica Acta (BBA) - Molecular Cell Research. 2011; 1813:1269–1278.

Schietinger A, Greenberg PD. Tolerance and exhaustion: defining mechanisms of T cell dysfunction. Trends Immunol. 2014; 35:51–60. [PubMed: 24210163]

Siska PJ, Rathmell JC. T cell metabolic fitness in antitumor immunity. Trends Immunol. 2015; 36:257–264. [PubMed: 25773310]

Spiegelman BM. Transcriptional control of energy homeostasis through the PGC1 coactivators. Novartis Foundation symposium. 2007; 286:3–6. discusssion 6–12, 162–163, 196–203. [PubMed: 18269170]

Staron MM, Gray SM, Marshall HD, Parish IA, Chen JH, Perry CJ, Cui G, Li MO, Kaech SM. The transcription factor FoxO1 sustains expression of the inhibitory receptor PD-1 and survival of antiviral CD8(+) T cells during chronic infection. Immunity. 2014; 41:802–814. [PubMed: 25464856]

Sukumar M, Liu J, Mehta GU, Patel SJ, Roychoudhuri R, Crompton JG, Klebanoff CA, Ji Y, Li P, Yu Z, et al. Mitochondrial Membrane Potential Identifies Cells with Enhanced Stemness for Cellular Therapy. Cell Metab. 2016; 23:63–76. [PubMed: 26674251]

van der Windt GJ, Everts B, Chang CH, Curtis JD, Freitas TC, Amiel E, Pearce EJ, Pearce EL. Mitochondrial respiratory capacity is a critical regulator of CD8+ T cell memory development. Immunity. 2012; 36:68–78. [PubMed: 22206904]

van der Windt GJ, O'Sullivan D, Everts B, Huang SC, Buck MD, Curtis JD, Chang CH, Smith AM, Ai T, Faubert B, et al. CD8 memory T cells have a bioenergetic advantage that underlies their rapid recall ability. Proc. Natl. Acad. Sci. USA. 2013; 110:14336–14341. [PubMed: 23940348]

Wenner CE. Targeting mitochondria as a therapeutic target in cancer. J. Cell. Physiol. 2012; 227:450–456. [PubMed: 21503875]

Wherry EJ, Kurachi M. Molecular and cellular insights into T cell exhaustion. Nat. Rev. Immunol. 2015; 15:486–499. [PubMed: 26205583]

Woo SR, Turnis ME, Goldberg MV, Bankoti J, Selby M, Nirschl CJ, Bettini ML, Gravano DM, Vogel P, Liu CL, et al. Immune inhibitory molecules LAG-3 and PD-1 synergistically regulate T-cell function to promote tumoral immune escape. Cancer Res. 2012; 72:917–927. [PubMed: 22186141]

Xiao B, Deng X, Zhou W, Tan E-K. Flow Cytometry-Based Assessment of Mitophagy Using MitoTracker. Front. Cell. Neurosci. 2016; 10:76. [PubMed: 27065339]

Zhao E, Maj T, Kryczek I, Li W, Wu K, Zhao L, Wei S, Crespo J, Wan S, Vatan L, et al. Cancer mediates effector T cell dysfunction by targeting microRNAs and EZH2 via glycolysis restriction. Nat. Immunol. 2015; 17:95–103. [PubMed: 26523864]

Highlights

- T cells infiltrating tumors show decreases in mitochondrial function and mass
- Loss of oxidative metabolism is specific to activation in the tumor microenvironment
- T cell mitochondrial biogenesis is repressed via Akt-mediated inhibition of PGC1α
- Enforced expression of PGC1α results in superior antitumor T cell function

In Brief

As the tumor microenvironment is nutrient-poor, the inability of T cells to attack and eliminate cancer cells might be linked to an inability to generate sufficient bioenergetic intermediates. Delgoffe and colleagues show that intratumoral T cells exhibit repressed mitochondrial metabolism and find that metabolically reprogramming T cells increases antitumor activity.

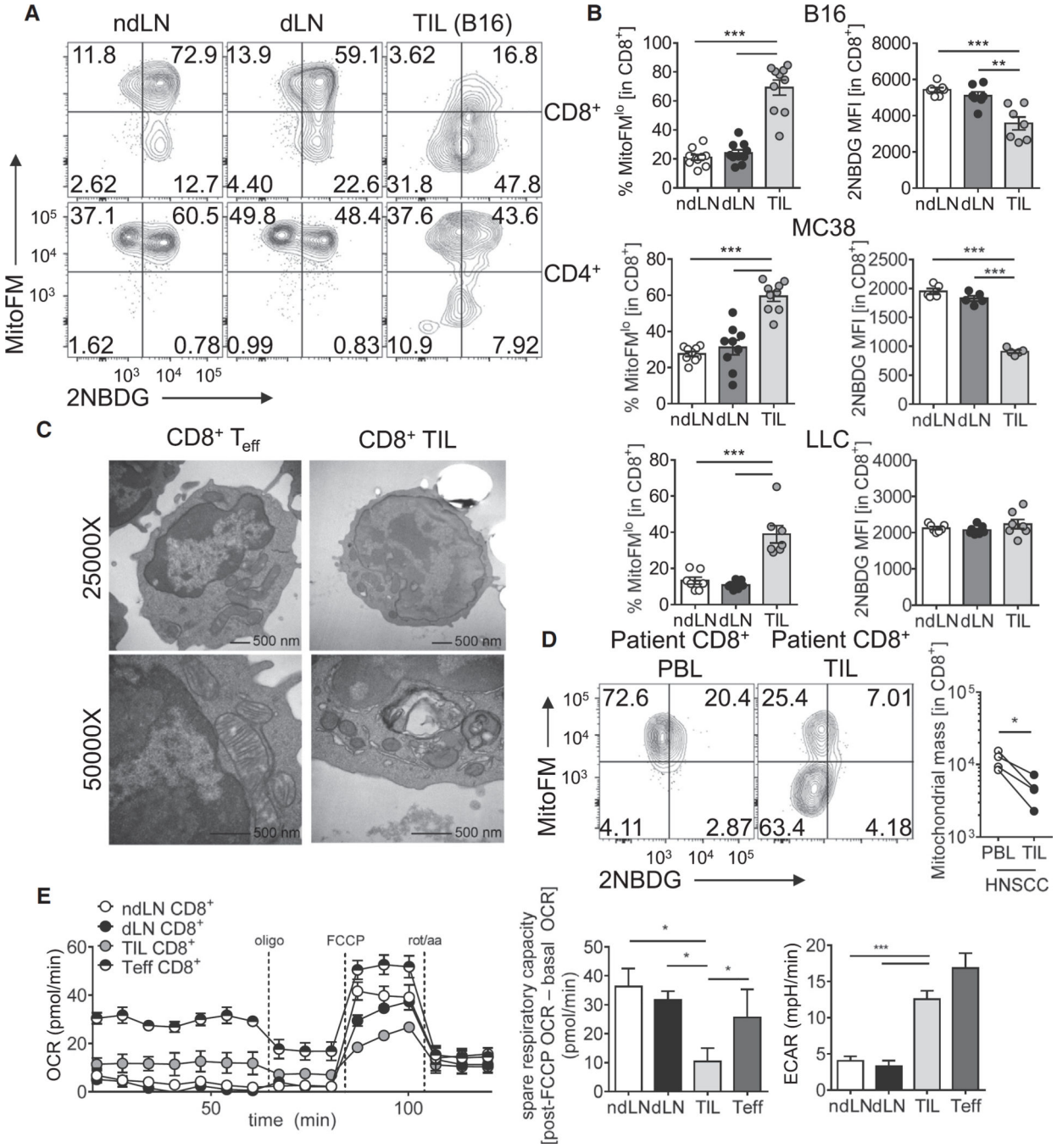

Figure 1. Tumor-Infiltrating CD8$^+$ T Cells Display Suppressed Mitochondrial Function and Mass

(A) Representative flow cytogram of nondraining (ndLN), draining (dLN) lymph node, or tumor-infiltrating lymphocyte (TIL) preparations from C57BL/6 mice inoculated with B16 melanoma cells 12 days prior, gated on CD8 or CD4 as indicated.

(B) Tabulated flow cytometric data from CD8$^+$ T cells isolated from mice bearing the indicated tumor types. Each circle represents an individual animal.

(C) Transmission electron microscopy of activated or tumor-infiltrating CD8$^+$ T cells.

(D) MitoTracker FM staining of $CD8^+$ T cells from peripheral blood lymphocyte (PBL) or TIL of HNSCC patients.

(E) Oxygen consumption rate (OCR) trace (left) and metabolic analysis panels (middle, right) from $CD8^+$ T cells isolated from the indicated sites from B16-bearing animals. T cells activated 24 hr with anti-CD3/anti-CD28 (Teff) are included as a control. Spare respiratory capacity (SRC) is calculated as the difference between initial, basal OCR values, and the maximal OCR values achieved after FCCP uncoupling. Data represent the mean or are representative of 3–5 independent experiments. *$p < 0.05$, **$p < 0.01$, ***$p < 0.001$ by unpaired t test. Error bars indicate SEM. See also Figure S1.

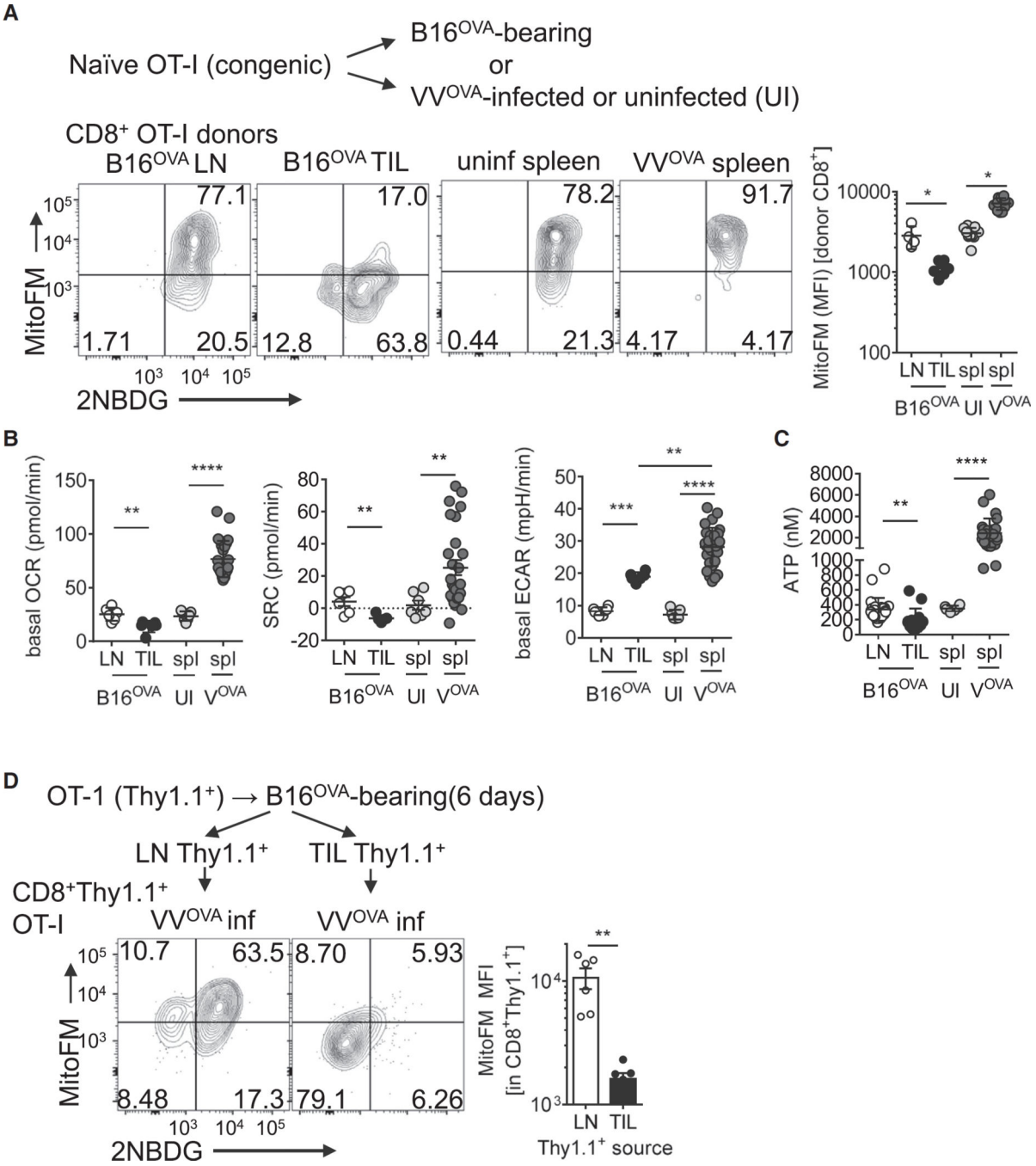

Figure 2. Loss of Mitochondrial Function and Mass Is Not Simply a Phenotype of Robust Activation In Vivo

(A) Representative flow cytogram and tabulated results of 2NBDG uptake and MitoTracker FM measurements of OT-I T cells injected into $B16^{OVA}$-bearing or VV^{OVA}-infected, or uninfected congenically mismatched hosts for 6 days. Plots are gated on $CD8^+$ T cells and the congenic allele marker (Thy1).

(B) Seahorse measurements (OCR, SRC, and ECAR) from cells in (A).

(C) ATP measurements from purified donor cells from (A).

(D) Flow cytogram of glucose uptake and mitochondrial mass of OT-I (Thy1.1^{+}) T cells adoptively transferred into B16^{OVA} bearing mice for 6 days, isolated from either LN or tumor, then transferred into VV^{OVA}-infected mice for 6 days. Flow cytogram depicts splenic CD8^{+}Thy1.1^{+} cells. *p < 0.05, **p < 0.01, ***p < 0.001 by unpaired ttest. Results represent four (A–C)or three (D) experiments. Circles represent individual animals. UI = uninfected V^{OVA}= VV^{OVA}-infected (1×10^{6} PFU IP), spl = spleen. Error bars indicate SEM. See also Figure S2.

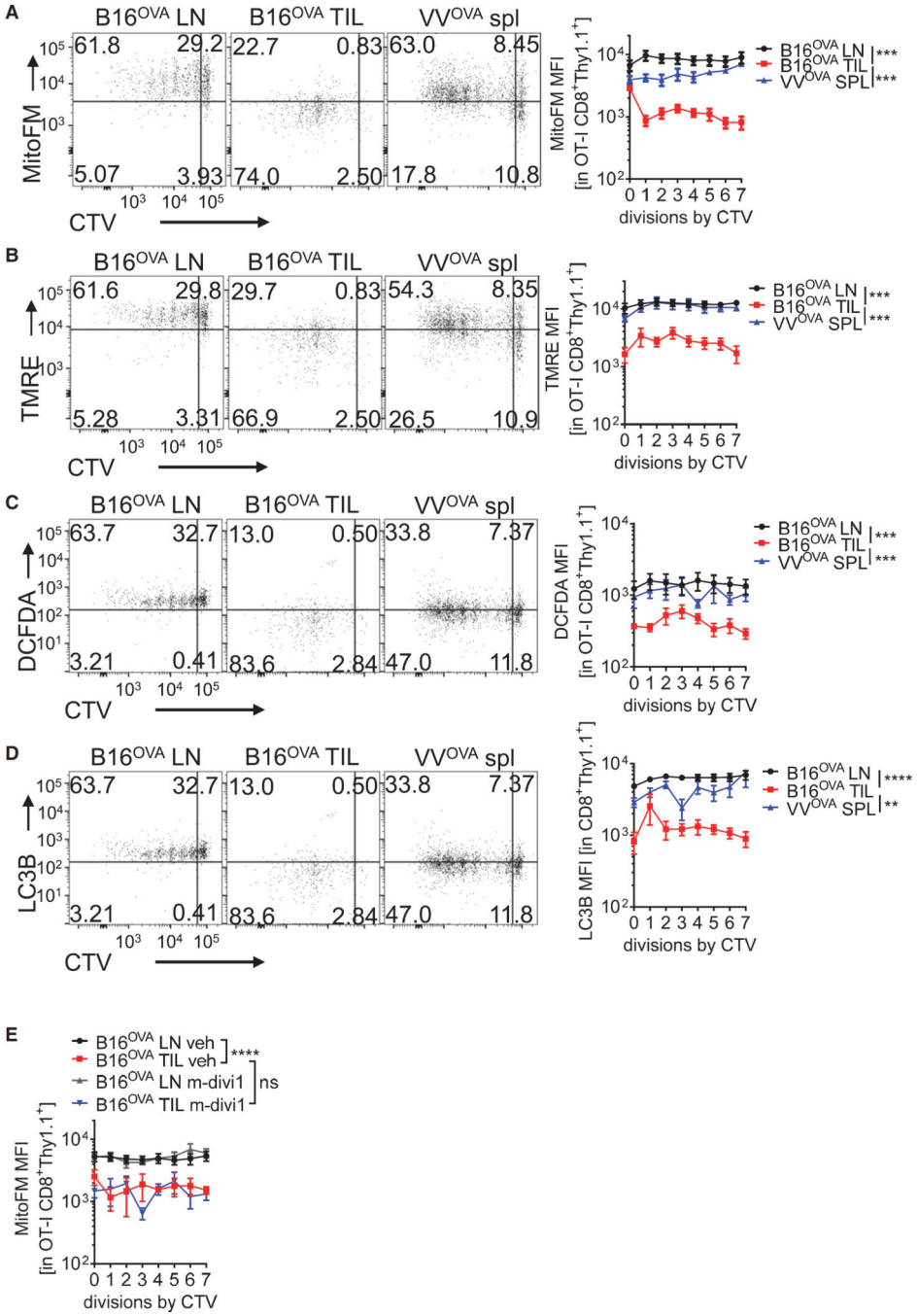

Figure 3. T Cell Mitochondrial Dysfunction Is Induced upon Entry into the Tumor Microenvironment

(A) Representative flow cytogram and tabulated data of LN and TIL of naive, CellTrace Violet (CTV)-labeled, OT-I (Thy1.1$^+$) CD8$^+$ T cells transferred into B16^{OVA}-bearing mice (5–7 mm tumors), or the spleens of the same progenitor cells transferred into B6 mice infected with 1 × 10^6 PFU VV^{OVA} for 72 hr. Cells were stained with MitoTracker Deep Red FM.

(B) As in (A), but with the mitochondrial membrane potential dye TMRE.

(C) As in (A), but with the cellular ROS indicator DCFDA.

(D) As in (A), but cells were permeabilized and stained intracellularly for LC3B.
(E) Representative data from experiments as in (A), but some mice received mitophagy inhibitor m-divi-1. Results represent the mean of three or four independent experiments, with n = 7–9 mice per group. **p < 0.01, ***p < 0.001, ***p < 0.0001 by two-way ANOVA. Error bars indicate SEM. See also Figure S3.

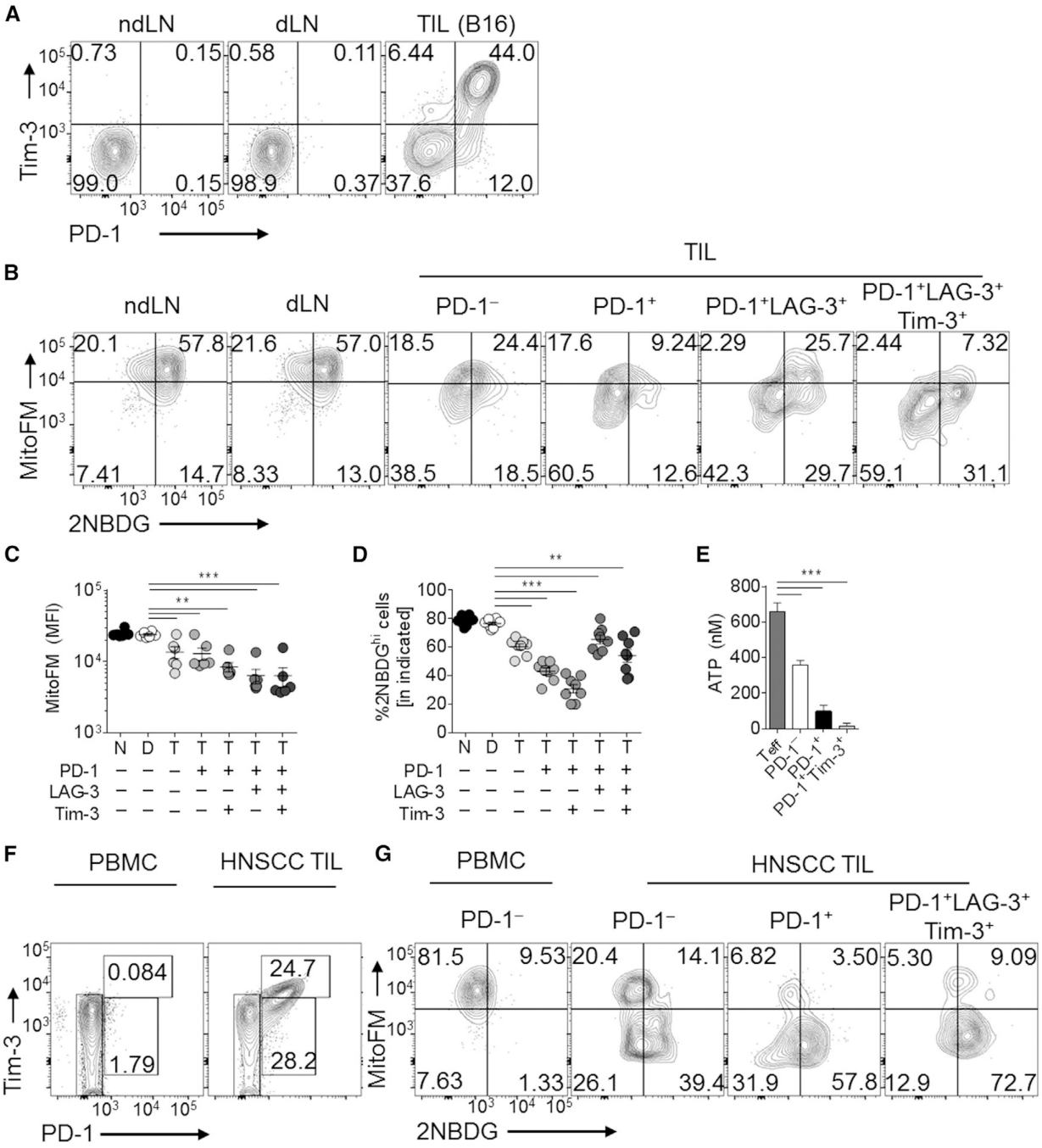

Figure 4. Mitochondrial Dysfunction in Intratumoral T Cells Is Progressive and Correlates with Coinhibitory Molecule Expression in Mouse and Human Tumors

(A) Representative flow cytogram of $CD8^+$ T cells isolated from day 14 B16-bearing C57/BL6 mice.

(B) Flow cytogram showing mitochondrial mass and glucose competency of $CD8^+$ T cell subsets. (C and D) Tabulated data from (B).

(E) ATP measurements from $CD8^+$ T cells sorted directly ex vivo from tumors based on the indicated expression. Results are compared to LN $CD8^+CD44^{hi}$ cells (Teff).

(F) Cytogram of coinhibitory molecules and (G) mitochondria/glucose status of $CD8^+$ cells from PBL or TIL from HNSCC patients. Data represent the mean or are representative of 3–5 independent experiments. *$p < 0.05$, **$p < 0.01$, ***$p < 0.001$ by unpaired t test. Error bars indicate SEM. See also Figure S4.

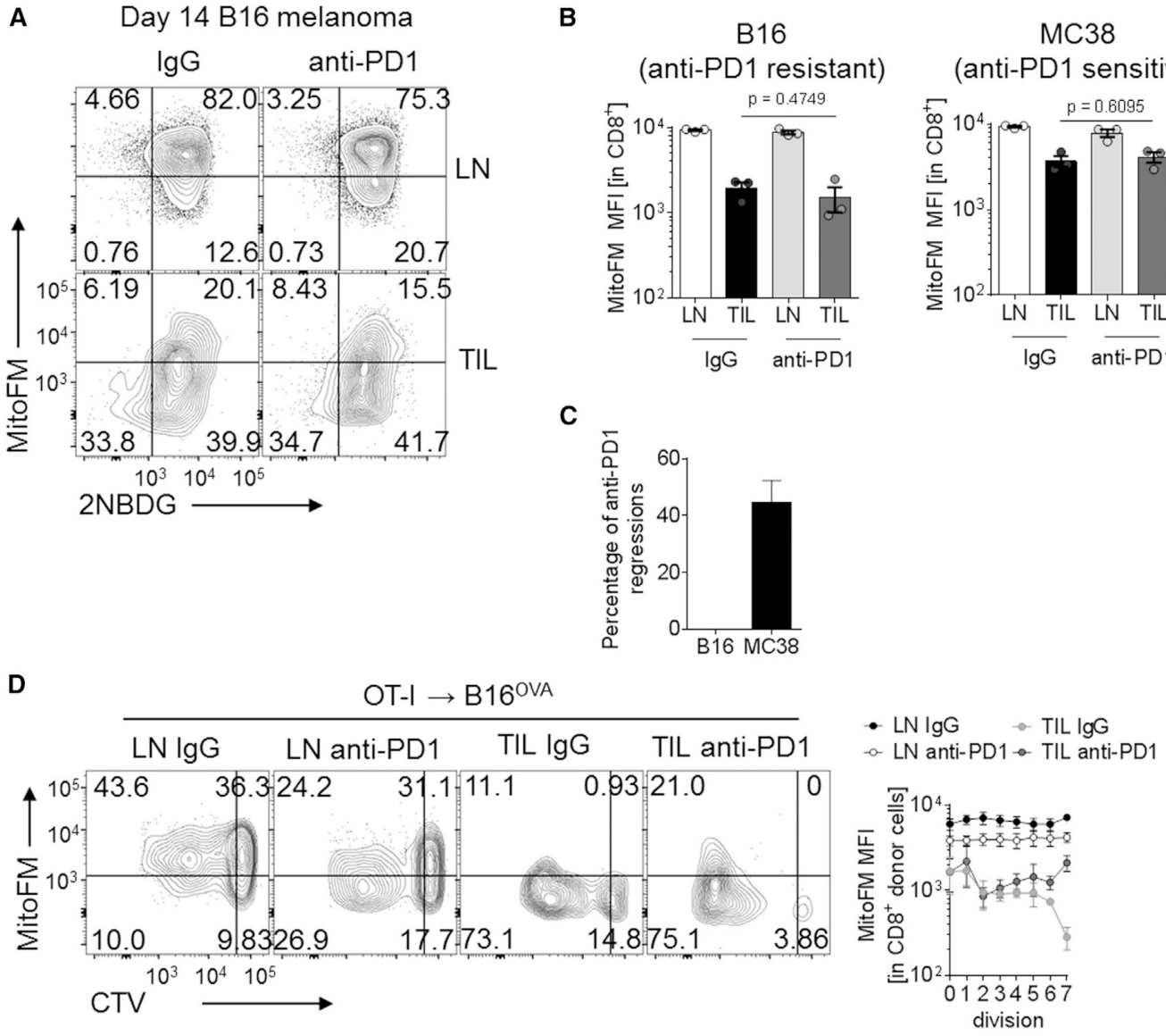

Figure 5. PD-1 Blockade Does Not Rescue Metabolic Dysfunction in Intratumoral T Cells

(A) Representative flow cytogram of $CD8^+$ T cells from LN and TIL preparations in B16-bearing mice receiving thrice-weekly injections of 200 μg anti-PD1 or its isotype control.

(B) Tabulated results from (A) as well as MC38-bearing mice. Each dot represents a mouse in this experiment.

(C) Percentage of mice experiencing tumor regression in several experiments conducted as in (B).

(D) Flow cytogram and tabulated values of MitoTracker FM staining during cell division of OT-I T cells transferred into established $B16^{OVA}$ tumors under the cover of anti-PD1 or its isotype control. Data are representative of five (A and B) or represent the mean of three (C and D) independent experiments. Error bars indicate SEM. See also Figure S5.

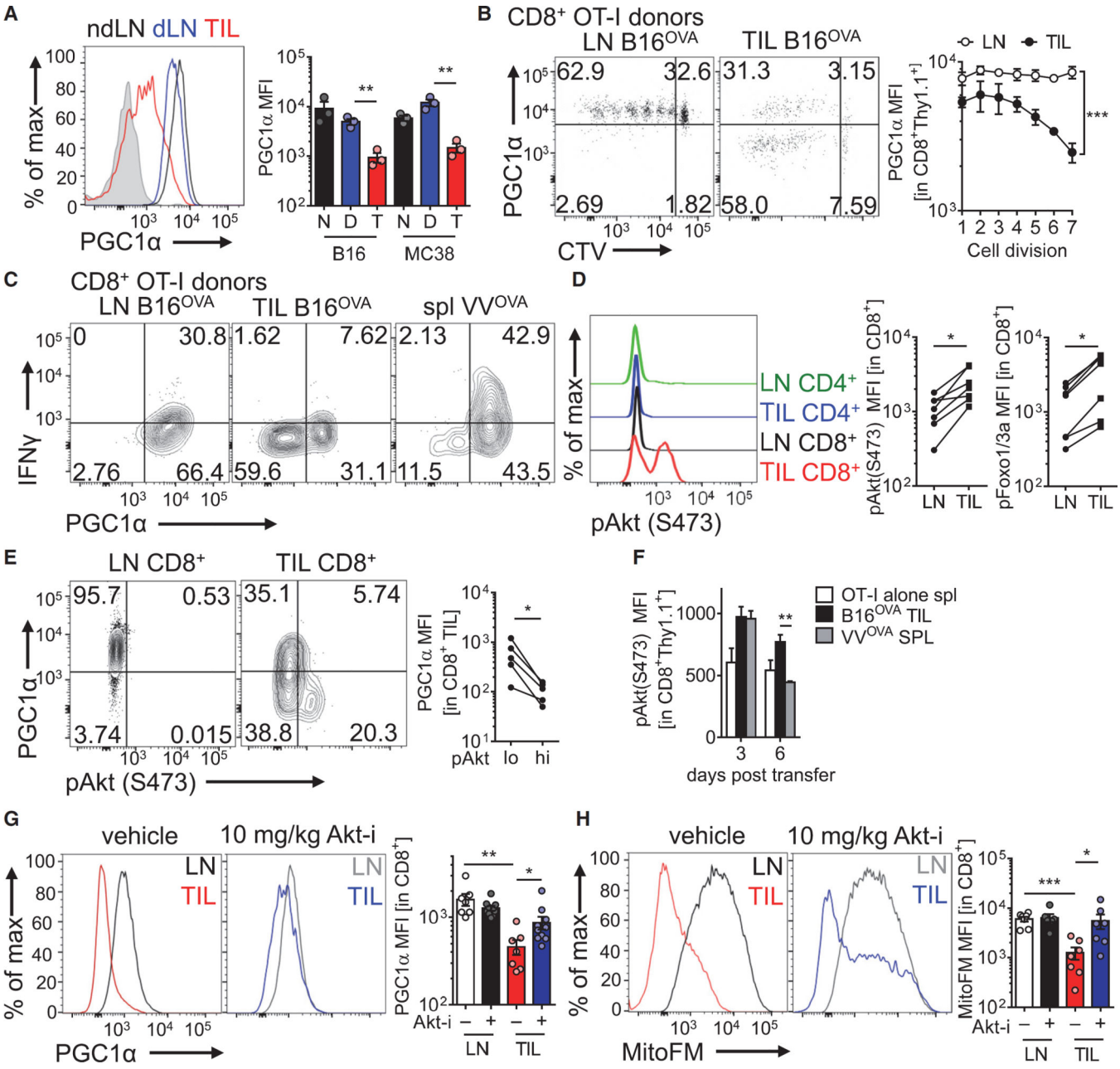

Figure 6. Intratumoral T Cell Mitochondrial Biogenesis Is Repressed by Chronic Akt-Mediated Repression of PGC1α

(A) Flow cytogram (left) and tabulated data (right) of PGC1α intracellular staining in CD8$^+$ T cells isolated from nondraining or draining LNs or TIL preparations from B16 or MC38 bearing mice. Shaded histogram indicates isotype control.

(B) Flow cytogram of PGC1α expression in CTV-labeled, naive OT-I T cells adoptively transferred into B16^{OVA} bearing mice for 72 hr. Tabulation for multiple experiments is to the right.

(C) Flow cytogram of cytokine production of congenically mismitached WT OT-I T cells transferred into $B16^{OVA}$-bearing or VV^{OVA}-infected mice for 96 hr, then restimulated with SIINFEKL peptide.
(D) Representative and tabulated phospho-Akt (S473) and phospho-Foxo1(T24)/3a(T32) staining of the indicated cell populations in mice bearing 14-day B16 tumors. MFI is reported.
(E) Representative flow cytogram and tabulated data indicating PGC1α staining in pAkt low or high cells.
(F) MFI of pAkt staining in naive OT-I T cells, or OT-I T cells transferred for 3 or 6 days into a $B16^{OVA}$-bearing or VV^{OVA} infected mouse.
(G) PGC1α levels and (H) mitochondrial mass of $CD8^+$ T cells from LN and TIL of 14-day B16-bearing mice treated for 60 hr with Akt inhibitor VIII or its vehicle. Results are representative of five (A, B, and D), three (C, E, G, and H), ortwo (F) independent experiments.*$p< 0.05$, **$p <0.01$, ***$p < 0.001$ by unpaired t test (A, F, G, and H) or paired t test (D, E, G, and H). ***$p < 0.001$ by two-way ANOVA. Error bars indicate SEM. See also Figure S6.

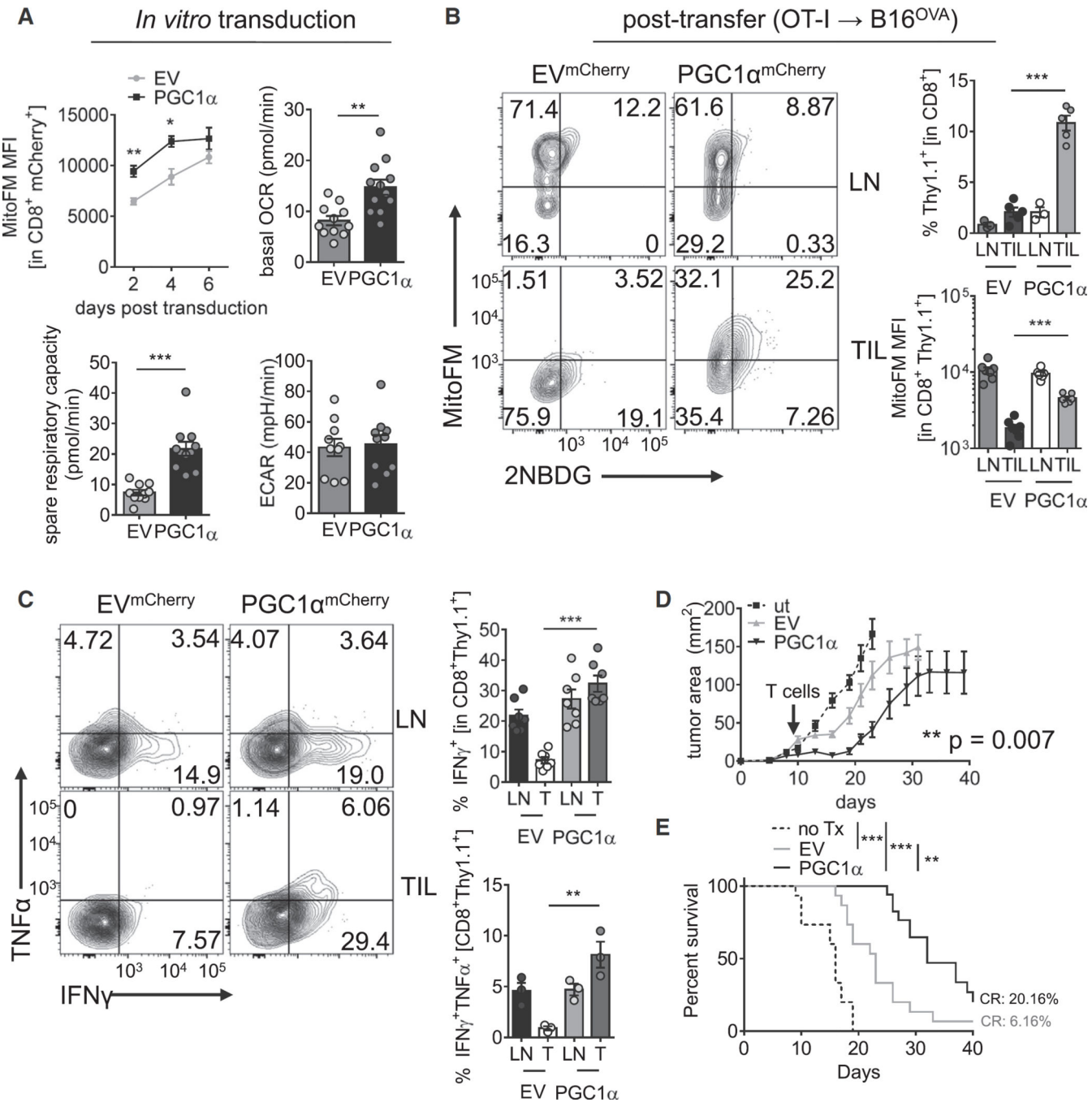

Figure 7. Bolstering Mitochondrial Biogenesis Improves Intratumoral T Cell Function

(A) Metabolic analysis of OT-I T cells retrovirally transduced with an empty mCherry vector (EV) or one encoding PGC1α. MitoTracker FM staining at various time points post transduction is indicated. OCR, SRC, and ECAR values are from day 5–7 post transduction. (B) Representative flow cytogram of LN- and TIL-resident OT-I T cells transduced as in (A) and transferred into $B16^{OVA}$ bearing C57/BL6 mice. Proportion of the transferred cells in LN and TIL and tabulated MitoTracker FM staining is reported.

(C) Flow cytogram depicting cytokine synthesis in OT-I T cells transferred as in (B) and restimulated directly ex vivo with cognate peptide. Results are tabulated to the right.
(D) Tumor growth plot of $B16^{OVA}$ bearing mice treated therapeutically upon detection of palpable tumors on day 7 with 250,000 (< $4mm^2$) or 500,000 (> $4mm^2$) of PGC1α or control-expressing cells.
(E) Survival plot from e.n = 15–17 mice per group. Results represent six (A and B), four (C), or three (D and E) independent experiments. **p < 0.01, ***p < 0.001 by unpaired t test (A–C), two-way ANOVA with repeated-measures (D), or log-rank test (E). Error bars indicate SEM. See also Figure S7.